

Project Outside of Course Scope

Head Movement in the Task-Based Functional Magnetic Resonance Imaging (fMRI)
Data of the Adolescent Brain Cognitive Development (ABCD) Study

Author: Jakob Flinck Sheye (zgh214)

Advisor: Melanie Ganz-Benjaminsen

Date: January 31, 2024

Contents

1	Introduction	4
2	Background	4
2.1	The ABCD Study	4
2.2	Magnetic Resonance Imaging	4
2.3	K-Space	5
2.4	Motion Artefacts	5
3	Methods	6
3.1	Head Motion Estimation	6
3.2	Euler Angles	6
3.3	Framewise Displacement	7
3.4	Data Acquisition	7
4	Results	9
5	Discussion	14
5.1	Standard Deviation	14
5.2	Statistical Significance	15
5.3	Outliers	15
5.4	Motion	15
5.5	Limitations & Further Work	15
6	Conclusion	16
7	Code Availability	16
8	Appendix	18

Abstract

In this project, baseline fMRI scans of 9-10 year old children are analysed in order to understand the prevalence and degree of head motion in children. The analysis focuses on subsets of resting-state fMRI data ($N = 9398$) and Emotional N-Back Task fMRI data ($N = 5357$) from the Adolescent Brain Cognitive Development study.

Decomposing the rigid body transformation matrices of each subject yields six displacement parameters; three translation parameters, and three rotation parameters. Each dataset is split by age and sex, and the distribution of the maximum absolute displacements is plotted as box-plots. Among the translation parameters, for both datasets, sexes, and age-groups, translation along the z -axis is found to be dominant, while rotation around the x -axis dominates the rotation parameters. Analysing the distributions show close to, or directly, overlapping means and medians, but a Kolmogorov-Smirnov test finds that the distributions are not normal. Furthermore, a Mann-Whitney U -test is evaluated across sex within each dataset for each displacement parameter in order to check for statistical significance. It is found, that statistical significance can be consistently observed between sex for distributions of translation along either one, or both, of the y -and- z axes. Finally, the standard deviation of each sub-population is also analysed across each dataset and motion. Across all displacement parameters, the standard deviation is found to decrease with age - with males having a higher standard deviation than females in the same age-group across both datasets. Interestingly, for males only, the standard deviation is found to decrease between resting-state fMRI and Emotional N-Back Task fMRI.

Taking limitations into account, these findings help illustrate how 9 and 10 year old children can be expected to move during resting-state fMRI scans and Emotional N-Back Task fMRI scans. Specifically, male children are found to move more than female children, with visual and active stimulation likely having a larger impact on decreasing movement in males.

1 Introduction

Head motion is the most frequent cause of artefacts in Magnetic Resonance Imaging (MRI) [4, 7]. Motion artefacts are a major concern, as they reduce image quality and may render images unusable, necessitating a new scan, further increasing costs, both monetary and time-wise. Especially children are prone to excessive motion, as they are more easily frightened by the narrow bore, huge machine, and loud noise [6]. Recently, functional MRI (fMRI) has seen an increased use in research on brain functioning in children [6]. fMRI is highly sensitive to movement [6, 13], hence it has become common practice to use either sedation or general anesthesia (GA) in young patients [4, 6, 7]. The use of GA and sedation comes with additional monetary costs, increases the patient’s waiting time, and concerns have been raised about possible adverse effects, such as airway obstruction [4, 6, 7].

In order to optimize the MRI acquisition for children in the clinical setting, insights into children’s motion patterns are essential. Understanding the prevalence and degree of head motion in children can help guide the development of motion correction techniques for MRI. This project aims to analyse the motion logs from subsets of the resting-state fMRI series and task-based fMRI series (EN-Back) of the Adolescent Brain Cognitive Development study to understand how far a typical child moves during scanning.

2 Background

2.1 The ABCD Study

The Adolescent Brain Cognitive Development (ABCD) study is the largest long-term study of brain development and child health in the United States [1]. The ABCD Research Consortium comprises a Coordinating Center, a Data Analysis, Informatics & Resource Center, and 21 research sites across the United States [1]. The ABCD study follows the brain development of 11,878 children aged 9–10 through adolescence (48% female; 52% male) into young adulthood [2]. The study aims to determine how experiences during childhood, such as smoking, sports and videogames, together with the changing biology of children, affect brain development [1]. As part of the ABCD study protocol multimodal neuroimaging of all participants is captured biannually [3], making it possible to analyse head motion across age and gender.

Participants (#)	Sex (F/M) (%)	Ethnicities (%)
11878	48/52	white (52.4%), black (13.4), hispanic (24.0%), asian (4.7%), mixed (4.2%), AIAN (0.8%), NHPI (0.2%), other (0.3%)

Table 1: Summary of the ABCD study population.

2.2 Magnetic Resonance Imaging

Magnetic Resonance Imaging (MRI) is a medical imaging technology often used in imaging of the brain. MRI is carried out by placing the participant in a strong external magnetic field, forcing the hydrogen protons, which are abundant in the human body, to align with the magnetic field [11, 14]. Bursts of a radio frequency (RF) pulse are then introduced, forcing the protons out of alignment with the magnetic field [11]. Once the RF pulse is turned off, the protons will realign with the magnetic field, releasing a signal in the form of electromagnetic energy, that can be detected by a receiver coil. Because digital computer processing of the data requires the released signal to be sampled at discrete times, the released signal must be sampled at appropriately frequent time intervals, defined as the Nyquist frequency [12]. In order to spatially encode the released signal, three magnetic gradient fields are considered. The field strengths of these magnetic fields depend linearly on the spatial position x , y , or z , respectively [14]. The purpose of the magnetic field gradients is twofold: 1) facilitating

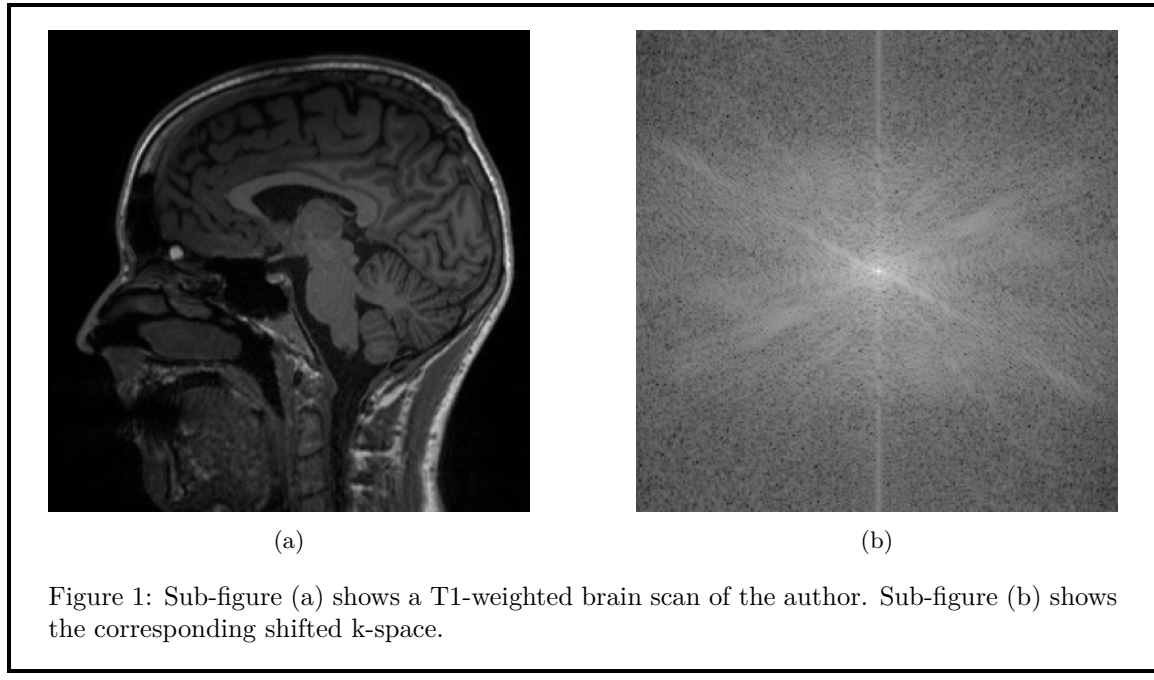
selective excitation of the nuclear spins in a partial body region, and 2) facilitating position encoding within an excited partial body region [14]. During scanning, the signals are written into k-space.

2.3 K-Space

MRI data acquisition occurs in k-space [17]. The k-space encodes the spatial frequencies of the imaged object in either two or three dimensions, depending on how the data is encoded [17]. In this project, for simplicity's sake, only the two-dimensional k-space will be considered. The k-space coordinates, k_x and k_y , are given by

$$k_x(t') = \int_0^{t'} \gamma G_x(t) dt \quad \text{and} \quad k_y(t') = \int_0^{t'} \gamma G_y(t) dt$$

where γ is the gyromagnetic ratio, $G(t)$ is the strength of the gradient as a function of time, and t' is the time at which the data sample is collected [12]. The individual k-space points do not correspond one-to-one with the points in the final image. Instead, each point in k-space contains information about all points in the final image, and each point in the final image maps to every point in k-space [10]. Thus, a change in a sample in k-space may affect the entire image, and vice versa [17]. The way each point in k-space affects the final image is determined by its placement in k-space. Points near the edge of k-space determine image resolution, while points near the center of k-space determine contrast in the final image [10]. The placement of points in k-space is controlled via gradient strength [10]. Thus, by manipulating the gradient strength that is applied during scanning, the resolution and contrast of the final image can be controlled. Finally, in order to reconstruct the image from the k-space, the inverse Fourier Transform is used [12]. Being able to control the data acquisition, manipulation, and reconstruction is what sets MRI apart from other medical imaging modalities [10].



2.4 Motion Artifacts

MRI scanning is a lengthy process, which is sensitive to motion. In MRI scans, human participants are prone to various types of motion, including periodic involuntary motion, such as breathing, sudden involuntary movements, such as sneezing or swallowing, and conscious motion caused by carelessness or discomfort [8]. Head motion is the most frequent cause of artefacts in MRI [4, 7], and

movement-induced artefacts typically manifest as ghosting, blurring or signal variation [7, 8]. Such artefacts may reduce the image quality and clinical relevance, as the artefacts can obstruct and even mimic pathologies [8]. Especially children struggle with excessive motion [6], making it relevant to optimize the MRI acquisition for children in the clinical setting.

3 Methods

3.1 Head Motion Estimation

Head motion estimation in an fMRI time-series involves spatially aligning, or registering, each volume of the series to a selected reference volume [13]. Thus, for each volume, the registration problem aims to find the rigid body transformation which maximizes the similarity between the transformed volume, $T(X)$, and the reference volume, Y . A common approach is to construct a cost function, $C(I_1, I_2)$, which quantifies the dissimilarity between two volumes and then search for the transformation which gives the minimum cost [9]. Thus

$$T^* = \arg \min_{T \in S_T} C(Y, T(X)) \quad (1)$$

where S_T is the space of rigid body transformations and T^* is the optimal transformation matrix.

Following Power et al. [13], each of the rigid body transformations can be expressed as a combination of rotation and displacement components, given by

$$T_i = \begin{bmatrix} R_i & d_i \\ 0 & 1 \end{bmatrix}$$

where R_i is a 3×3 rotation matrix, d_i is a 3×1 column vector of displacements, and i indexes volume corresponding to X in equation (1). The fourth row of T_i is the row vector $[0 \ 0 \ 0 \ 1]$ which is added to ensure that T_i has an inverse, guaranteeing each motion can be undone. Furthermore, R_i is composed of three elementary rotations around the x , y and z -axes. It is standard practice to first consider the rotation around the z -axis, then the y -axis, and finally the x -axis. Thus $R_i = R_{i\alpha}R_{i\beta}R_{i\gamma}$, and

$$R_{i\alpha} = \begin{bmatrix} 1 & 0 & 0 \\ 0 & \cos \alpha_i & -\sin \alpha_i \\ 0 & \sin \alpha_i & \cos \alpha_i \end{bmatrix}, \quad R_{i\beta} = \begin{bmatrix} \cos \beta_i & 0 & \sin \beta_i \\ 0 & 1 & 0 \\ -\sin \beta_i & 0 & \cos \beta_i \end{bmatrix},$$

$$R_{i\gamma} = \begin{bmatrix} \cos \gamma_i & -\sin \gamma_i & 0 \\ \sin \gamma_i & \cos \gamma_i & 0 \\ 0 & 0 & 1 \end{bmatrix}$$

where α_i , β_i and γ_i are the rotation angles in radians around the x , y and z -axes, respectively. Similarly, d_i consists of three elementary displacements along each axis, and is given by

$$d_i = \begin{bmatrix} d_{ix} \\ d_{iy} \\ d_{iz} \end{bmatrix}$$

It follows, that each rigid body transformation has three translation parameters, d_x , d_y and d_z , and three rotation parameters, α , β and γ - equalling a total of six degrees of freedom. In this paper, the rotation parameters were computed as the Euler angles.

3.2 Euler Angles

Consider the general rotation matrix

$$R = \begin{bmatrix} R_{11} & R_{12} & R_{13} \\ R_{21} & R_{22} & R_{23} \\ R_{31} & R_{32} & R_{33} \end{bmatrix}$$

Recall that the rotation matrix is composed of three elementary rotations

$$R = R_\alpha R_\beta R_\gamma$$

where

$$R = \underbrace{\begin{bmatrix} 1 & 0 & 0 \\ 0 & \cos \alpha & -\sin \alpha \\ 0 & \sin \alpha & \cos \alpha \end{bmatrix}}_{R_\alpha} \underbrace{\begin{bmatrix} \cos \beta & 0 & \sin \beta \\ 0 & 1 & 0 \\ -\sin \beta & 0 & \cos \beta \end{bmatrix}}_{R_\beta} \underbrace{\begin{bmatrix} \cos \gamma & -\sin \gamma & 0 \\ \sin \gamma & \cos \gamma & 0 \\ 0 & 0 & 1 \end{bmatrix}}_{R_\gamma}$$

Computing the matrix product $R = R_\alpha R_\beta R_\gamma$ yields

$$\begin{bmatrix} \cos(\beta) \cos(\gamma) & -\cos(\beta) \sin(\gamma) & \sin(\beta) \\ \sin(\alpha) \sin(\beta) \cos(\gamma) + \cos(\alpha) \sin(\gamma) & \cos(\alpha) \cos(\gamma) - \sin(\alpha) \sin(\beta) \sin(\gamma) & -\sin(\alpha) \cos(\beta) \\ \sin(\alpha) \sin(\gamma) - \cos(\alpha) \sin(\beta) \cos(\gamma) & \cos(\alpha) \sin(\beta) \sin(\gamma) + \sin(\alpha) \cos(\gamma) & \cos(\alpha) \cos(\beta) \end{bmatrix}$$

The Euler angles are then computed by equating the components of the general rotation matrix with those of the matrix product [15]

$$\begin{aligned} R_{13} &= \sin(\beta) \Leftrightarrow \beta = \arcsin(R_{13}) \\ \frac{R_{12}}{R_{11}} &= -\frac{\cos(\beta) \sin(\gamma)}{\cos(\beta) \cos(\gamma)} = -\tan(\gamma) \Leftrightarrow \gamma = -\arctan\left(\frac{R_{12}}{R_{11}}\right) \\ \frac{R_{23}}{R_{33}} &= -\frac{\sin(\alpha) \cos(\beta)}{\cos(\alpha) \cos(\beta)} = -\tan(\alpha) \Leftrightarrow \alpha = -\arctan\left(\frac{R_{23}}{R_{33}}\right) \end{aligned}$$

where α, β and γ are in radians. In theory, using Euler angles may result in division by zero due to a Gimbal lock. This corresponds to a loss in the degrees of freedom. In head motion, a Gimbal lock should not be able to occur given the natural constraints on the movement of the neck. In practice, to avoid any unspecified behaviour, a term ϵ corresponding to machine epsilon was added to R_{11} and R_{33} if they equalled zero.

3.3 Framewise Displacement

Framewise displacement is a motion measure that quantifies instantaneous head motion by expressing the change in head position between frames. Framewise displacement is computed using the formula

$$FD_i = |\Delta d_{ix}| + |\Delta d_{iy}| + |\Delta d_{iz}| + |\Delta \alpha_i| + |\Delta \beta_i| + |\Delta \gamma_i|$$

where $\Delta d_{ix} = d_{(i-1)x} - d_{ix}$, and likewise for the other translation and rotation parameters. Following the approach by Power et al. [13], the rotation parameters are converted to millimeters by calculating the displacement on the surface of a sphere of radius 50 mm, which is approximately the mean distance from the cerebral cortex to the center of the head. The conversion is carried out using the great-circle distance, which is computed as

$$d = r\Delta\sigma$$

where r is the radius, and $\Delta\sigma$ is the central angle in radians, corresponding to the rotation parameters, α, β and γ .

3.4 Data Acquisition

Within this project, subsets of year 1 baseline resting-state fMRI (rs-fMRI) data and task-based fMRI data acquired in the ABCD study were analyzed. The ABCD study imaging data acquisition protocol is based on a pilot-study of over 30 children [5]. Following this protocol, a scan session consists of a fixed order of scan types, starting with a localizer, acquisition of 3D T1w images, 2 runs of resting state fMRI, diffusion weighted images, 3D T2w images, 1-2 more runs of rs-fMRI, and the task-based fMRI [5]. The task-based fMRI consists of three tasks; 1) Monetary Incentive Delay Task, 2) Stop Signal Task, and 3) Emotional N-Back Task (EN-Back). The ordering of these tasks was randomized across subjects during acquisition. This project kept its focus on the EN-Back Task in the analysis of task-based fMRI.

Table 2: An abridged version of the ABCD baseline protocol brochure's page 9, available here: https://abcdstudy.org/wp-content/uploads/2019/12/Brochure_Protocol-Baseline-eg.pdf. Legend: - children were not distracted during the scan, - children were shown a movie, - children were solving a task.

Scan module	Protocol	Runs	Duration (min)	Distraction
Scan (inside scanner)	Set-up	-	3-6	
	rs-fMRI	2-5	10 (max)	
	DTI	1	9-10	
	rs-fMRI	2-5	10 (max)	
	EN-Back Task	2	12 (max)	

The EN-Back Task is designed to activate core brain networks relevant for working memory [5]. Hence, the EN-Back Task is used as a measure of emotion reactivity, utilizing a set of happy, fearful and neutral faces as stimuli. In the ABCD study, the EN-Back Task is programmed as an eight-block design with four blocks of 2-back conditions and four blocks of 0-back conditions [5]. The task included two runs of eight blocks each. The N-Back conditions are summarized in the following:

- **2-Back:** The participant is instructed to respond "match" when the current stimuli is the same as the one shown two trials back.
- **0-Back:** The participant is instructed to respond "match" when the current stimuli is the same as the one shown in the beginning of the block.

Comparably, in the resting-state scans, the participants were instructed to look in the general direction of a fixation crosshair [5].

Before entering the scanner, the participants undergo simulation and compliance training. This includes simulating scan sessions in a mock scanner and practicing the fMRI tasks in order to ensure they are familiar with the scanner environment, and understand the task instructions [5].

The ABCD study registers subject age in months, yet considers the age of the subjects as the year of the scan minus the year of birth (of the subject). Consequently, some children may be eight or eleven years old at the date of their scan. Within this project, only the children who were aged 9 or 10 at the date of their scan were considered. After scrubbing the subsets, the rs-fMRI dataset consisted of 9398 participants (47.6% female; 52.4% male), and the EN-Back Task fMRI dataset consisted of 5357 participants (48.7% female; 51.3% male).

	rs-fMRI				EN-Back Task fMRI			
	9-yo m	9-yo f	10-yo m	10-yo f	9-yo m	9-yo f	10-yo m	10-yo f
Participants	2509	2358	2415	2116	1372	1378	1369	1238

Table 3: Summary of participant numbers across fMRI scan activities. Each activity is split by participant age and sex.

4 Results

Motion curves of a randomly selected 9-year old female are visualized in figure 2. Sub-figure (c) visualizes the relationship between the motion curves and the axial orientation of the brain. It is assumed the z -axis of the scanner is flipped, hence positive translation along the z -axis corresponds to the subject sliding out of the scanner.

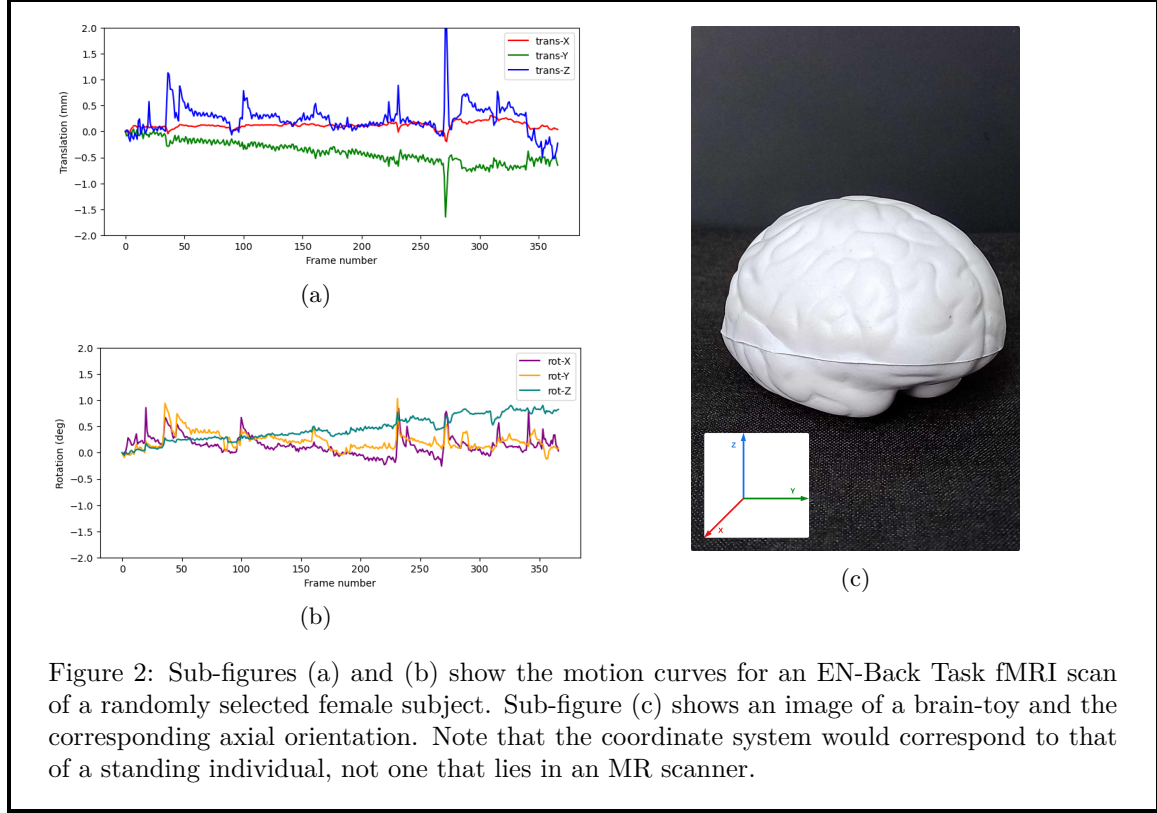


Figure 2: Sub-figures (a) and (b) show the motion curves for an EN-Back Task fMRI scan of a randomly selected female subject. Sub-figure (c) shows an image of a brain-toy and the corresponding axial orientation. Note that the coordinate system would correspond to that of a standing individual, not one that lies in an MR scanner.

Processing of the rs-fMRI data and EN-Back Task fMRI data was performed the same for both. For each dataset, the maximum absolute displacement of all translation and rotation parameters was computed. The distribution of the maximum absolute displacements, split by dataset, age and sex, was plotted as boxplots in figures 3-10.

Motion	rs-fMRI				EN-Back Task fMRI			
	9-yo m	9-yo f	10-yo m	10-yo f	9-yo m	9-yo f	10-yo m	10-yo f
trans-X	3.173	2.806	2.784	2.358	3.006	2.731	2.598	2.457
trans-Y	7.414	6.891	6.026	4.439	6.39	6.250	5.076	4.842
trans-Z	8.674	7.888	7.357	6.401	7.445	7.214	6.622	5.756
rot-X	10.691	9.342	8.978	7.515	10.272	8.568	8.091	7.374
rot-Y	3.972	3.41	3.532	2.9	4.144	3.497	3.15	3.67
rot-Z	5.656	4.796	4.673	3.944	4.992	4.654	4.439	4.058

Table 4: Summary of sub-populations' standard deviation across different activities and motions. All values are rounded to the third decimal digit.

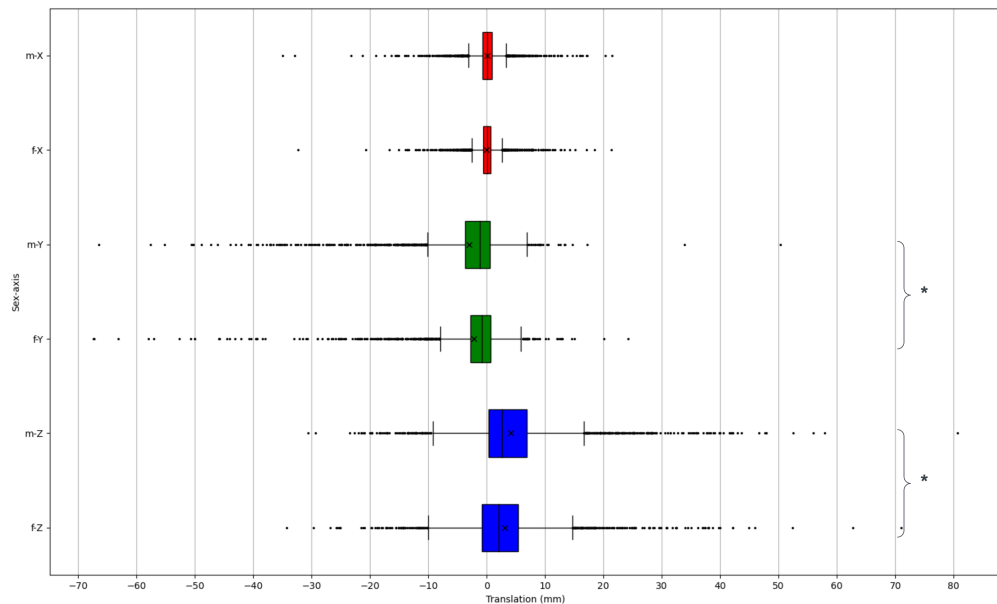


Figure 3: (rs-fMRI) Boxplot of maximum absolute translation displacements (mm) for 9-year old children. Statistical significance ($p < 0.001$) is indicated by *. Mean is indicated by \times .

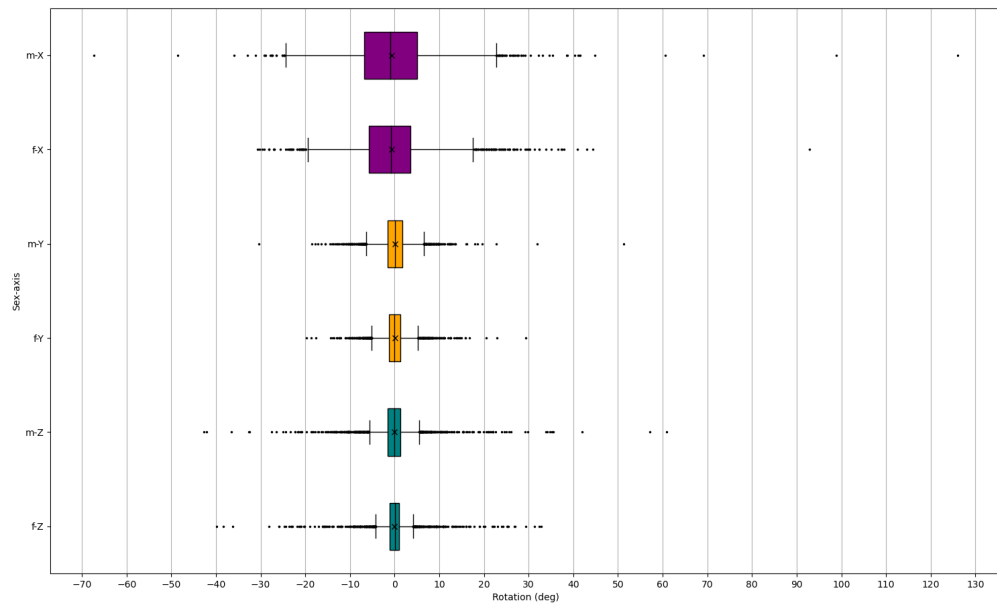


Figure 4: (rs-fMRI) Boxplot of maximum absolute rotation displacements (deg) for 9-year old children. Mean is indicated by \times .

Sex	Trans-X	Trans-Y	Trans-Z	Rot-X	Rot-Y	Rot-Z
Male	402	286	260	71	233	390
Female	399	280	224	128	261	372

Table 5: (rs-fMRI) Outliers, 9-year old children.

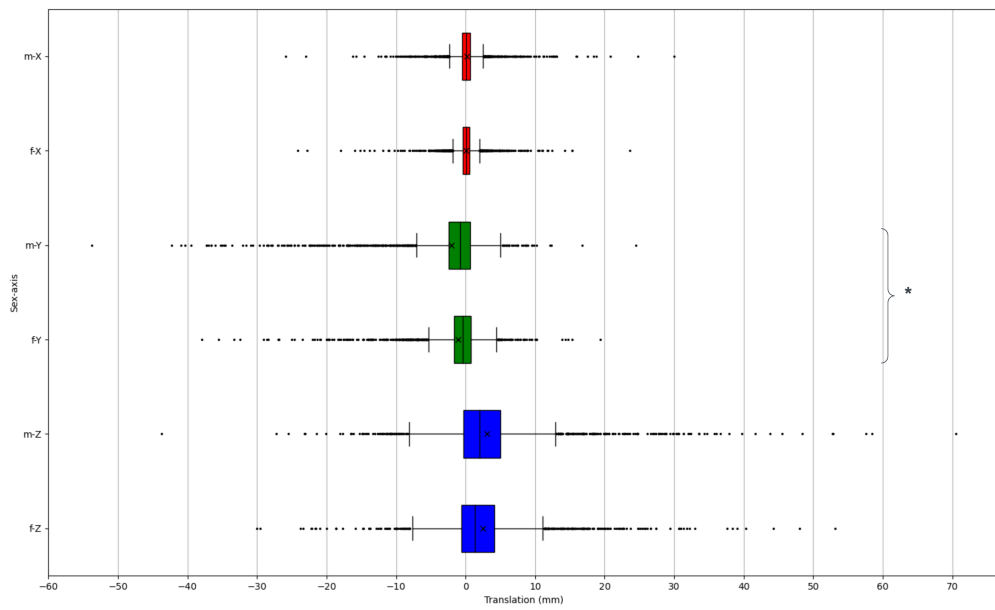


Figure 5: (rs-fMRI) Boxplot of maximum absolute translation displacements (mm) for 10-year old children. Statistical significance ($p < 0.001$) is indicated by *. Mean is indicated by \times .

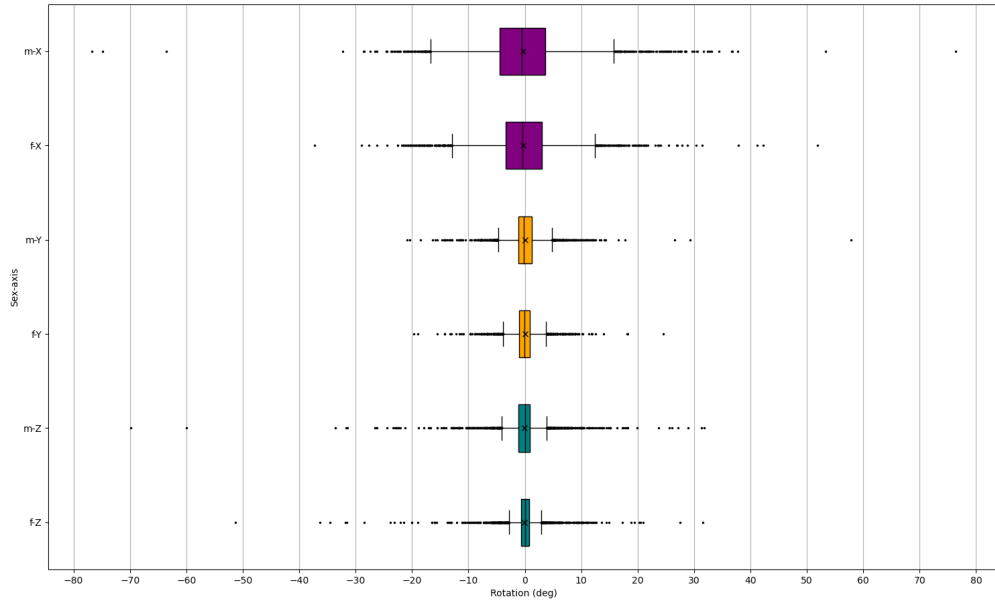


Figure 6: (rs-fMRI) Boxplot of maximum absolute rotation displacements (deg) for 10-year old children. Mean is indicated by \times .

Sex	Trans-X	Trans-Y	Trans-Z	Rot-X	Rot-Y	Rot-Z
Male	396	286	227	169	257	398
Female	383	267	206	207	269	388

Table 6: (rs-fMRI) Outliers, 10-year old children.

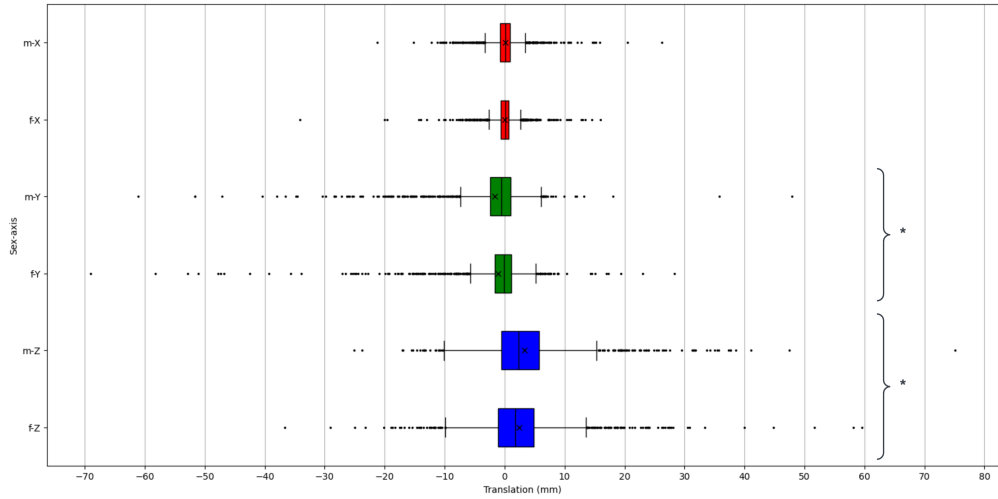


Figure 7: (EN-Back Task fMRI) Boxplot of maximum absolute translation displacements (mm) for 9-year old children. Statistical significance ($p < 0.001$) is indicated by *. Mean is indicated by \times .

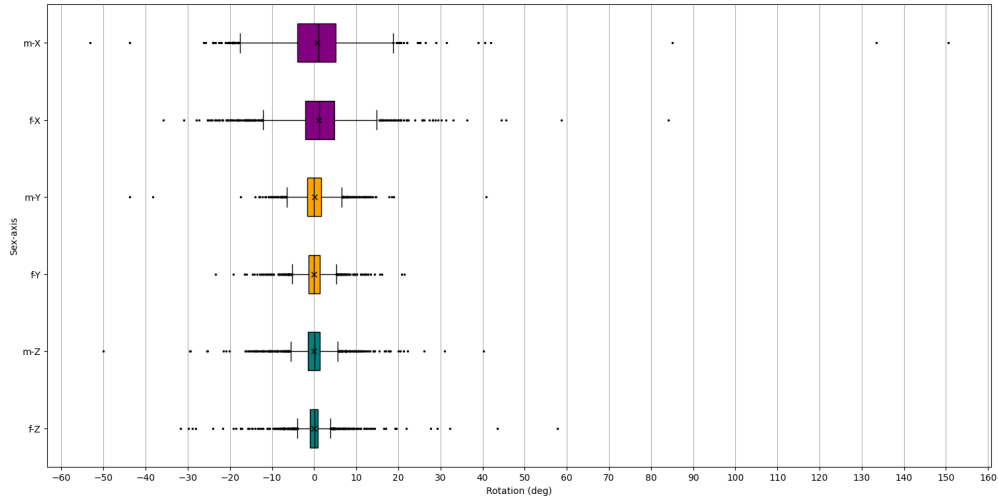


Figure 8: (EN-Back Task fMRI) Boxplot of maximum absolute rotation displacements (deg) for 9-year old children. Mean is indicated by \times .

Sex	Trans-X	Trans-Y	Trans-Z	Rot-X	Rot-Y	Rot-Z
Male	203	155	93	56	110	186
Female	226	164	117	140	144	233

Table 7: (EN-Back Task fMRI) Outliers, 9-year old children.

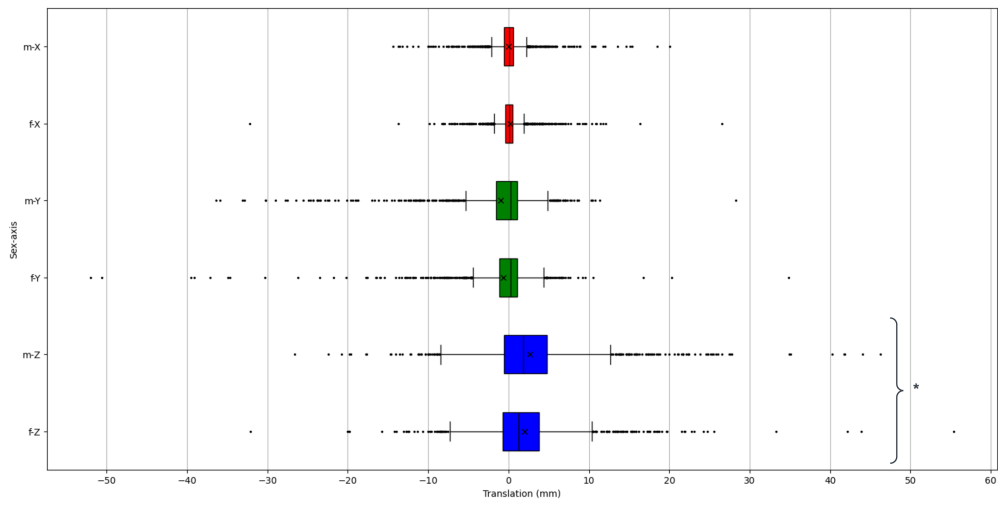


Figure 9: (EN-Back Task fMRI) Boxplot of maximum absolute translation displacements (mm) for 10-year old children. Statistical significance ($p < 0.001$) is indicated by *. Mean is indicated by \times .

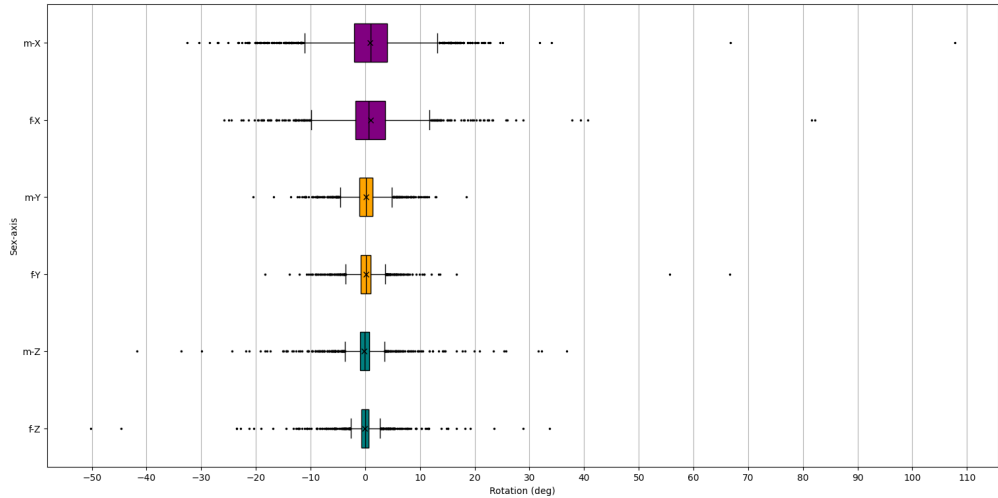


Figure 10: (EN-Back Task fMRI) Boxplot of maximum absolute translation displacements (deg) for 10-year old children. Mean is indicated by \times .

Sex	Trans-X	Trans-Y	Trans-Z	Rot-X	Rot-Y	Rot-Z
Male	248	179	124	149	154	228
Female	234	156	110	118	172	221

Table 8: (EN-Back Task fMRI) Outliers, 10-year old children.

The number of outliers in each boxplot is summarized in tables 5-8. For rs-fMRI it was found that males tend to have more outliers than females, regardless of age. For EN-Back Task fMRI it was found that 9-year old females have more outliers across all displacement parameters than the males in the same age-group. Interestingly, 10-year old females had less outliers than the males across all displacement parameters, except for the rotation along the y -axis.

In figures 3-10 it was observed across datasets, age and sex, that the interquartile range was largest for the translation along the z -axis, followed by the translation along the y -axis, with the translation along the x -axis having the smallest interquartile range. Interestingly, and also across datasets, age and sex, this ordering was reversed for the rotation displacements. Furthermore, it was observed that the means and medians of all displacement parameters, across dataset, age and sex, were either close to, or directly, overlapping. Therefore, it was found relevant to test the distributions for normality. A Kolmogorov-Smirnov test was evaluated for each displacement, and it was found that none of the displacements were normal distributed. A subset of the distributions is visualized as a histogram in figure 11. Using the mean and standard deviation of the distributions, the theoretical normal distributions are visualized on top of the histograms, clearly illustrating, that the distributions are not normal.

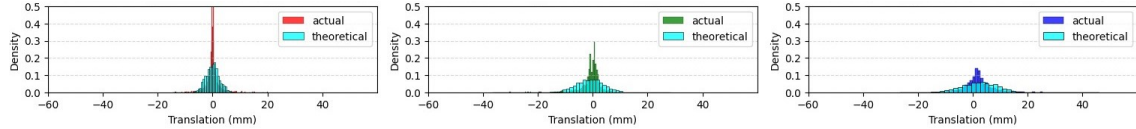


Figure 11: Visualizing the distributions of maximum absolute translation displacement for 10-year old males (EN-Back Task fMRI) with theoretical normal distributions overlaid.

In order to check for statistical significance, a Mann-Whitney U -test was evaluated across sex within each dataset and displacement parameter. The Mann-Whitney U -test was picked specifically, because the Kolmogorov-Smirnov test showed that the distributions were not normal. Displacements that were found to have statistical significance are marked with an asterisk (*) in figures 3-10.

The standard deviation for each displacement parameter is visualized across datasets, age and sex, in table 4. Across all displacements parameters, the standard deviation was found to decrease with age within datasets and sex. Males were found to have a higher standard deviation than females in the same age-group across both datasets, with the only exception being found at rotation around the y -axis in EN-Back Task fMRI.

5 Discussion

5.1 Standard Deviation

There are multiple observations to discuss regarding the standard deviations. First, males having a higher standard deviation than their female counterparts is in line with prior research [4, 16]. Second, younger children moving more than older children is not that surprising, and was also observed in [16]. Third, following Yuan et. al [16], tasks that involve active responses and multi-sensory stimulation appear less susceptible to head motion than tasks that do not include a visual component or active responses. Comparing the standard deviations across datasets, within age and sex, shows that the standard deviation decreases between rs-fMRI and Emotional N-Back Task fMRI for males - with rotation around the z -axis being the only outlier for 9-year old males. Interestingly, the same observation does not hold true for females. In this comparison it is important to note the different sizes of the datasets, as well as realizing that there is not a 100% overlap between the children in the larger dataset and the smaller dataset. Nonetheless, this observation could indicate that visual and active stimulation has a larger effect on males than females.

5.2 Statistical Significance

Within each dataset and age-group, statistical significance was consistently observed between sex for distributions of translations along either one, or both, of the y -and- z axes. This observation emphasizes that males tend to move more than females within the bore, regardless of what activity they are doing within the scanner. The fact that no statistical significance is found between sex for distributions of translations along the x -axis is likely related to the observation, that the x -translation has the smallest interquartile range. It is common practice to place padding on both sides of the subject's head, significantly limiting the range of possible motion along the x -axis. It is theorized the use of padding is the reason no statistical significance is observed for translations along the x -axis.

Interestingly, no statistical significance was found among the distributions of the rotations. This may be a result of the children adjusting their head to get a better view of either the crosshair in the resting-state scan, or task visualization, in the task-based scan. Assuming the head size is about the same for both sexes, the angle the children had to turn their head would be about the same.

5.3 Outliers

In the rs-fMRI scans, where no stimulation is present, males were found to have more outliers than females across both age-groups. This is in agreement with the findings in [16], who found that boys in general move more than girls for tasks that do not involve a visual system.

Comparably, it was found in the EN-Back Task fMRI scans, that 9-year old females had more outliers than males, while 10-year old females had less outliers than their male counterparts. Recall, that the task-based fMRI scans were last in the scan protocol. One explanation could be, that at the time of the EN-Back Task fMRI scans, the children were experiencing fatigue from the time spent in the scanner, making them more prone to moving around, regardless of sex or age. Hence, this observation could be interpreted as noise in the data.

5.4 Motion

Across both datasets, the distribution of the z -axis translations was found to have the largest interquartile range. This observation can likely be explained by drift motion, simply meaning the children are sliding out of the bore. Similar observations were made in [7]. Similarly, the distribution of the y -axis translations can be interpreted as the children sinking into the pillow their head is resting on. This, together with the z -axis translations, can be interpreted as the their head moving away from the more padded middle of the pillow, and towards the less padded edges, as they slide outwards of the bore, causing their head to sink. The small interquartile range observed for the x -axis translations is likely to be explained by the use of padding on the side of the head. Such padding severely reduces the range of possible motions along the x -axis within the bore.

Across both datasets, the distribution of the x -axis rotations was found to have the largest interquartile range. Rotation around the x -axis corresponds to nodding, which is a relatively unrestricted motion within the bore. Its larger range may be a result of the children adjusting their head to get a better view of either the crosshair in the resting-state scan, or task visualization, in the task-based scan. Comparatively, the distribution of the y -and- z axis rotations had small interquartile ranges. This could be explained by the use of padding on the side of the head, which restricts both y -axis rotation and z -axis rotation, corresponding to rolling and turning, respectively.

5.5 Limitations & Further Work

This project does have its limitations. First of all, there is a large difference in the size of the two datasets making it difficult to draw conclusions across them. Secondly, there is the question of scanner fatigue. Since the task-based fMRI scans were last in the protocol, it seems reasonable to argue, that the measured displacement magnitudes are inflated in these scans, as the children will tire out after spending a long time in the bore. In relation hereto, it was found, that some

children had upwards of eight runs, while others had two to three. This might be due to the children requesting a run be stopped, cutting it short, or other external factors. It might be interesting to research whether there is any relationship between the number of runs and the magnitude of the displacements. It seems reasonable to believe that children might move more in later runs, as they get tired out and uncomfortable in the scanner.

It is important to keep in mind, that the children were desensitized to the scanner environment beforehand. This is likely to have had a sizeable influence on the magnitude of the motions registered within the scanner. Hence, these findings may not generalize well to children who have not had prior experience with MR scans.

Further work could extend upon these observations by including the full baseline datasets, and looking into any correlations between the number of runs and the largest magnitude of the displacement parameters. Furthermore, it would also be interesting to analyse the correlation between displacement parameters. For example, if there indeed is a correlation between sliding out of the scanner, corresponding to positive translation displacement along the z -axis, and sinking into the pillow, corresponding to negative translation displacement along the y -axis.

6 Conclusion

Taking into account the discussed results and limitations, this study sheds some light on how 9 and 10-year old children can be expected to move during resting-state fMRI scans and Emotional N-Back Task fMRI scans. By analysing distributions of maximum absolute displacement parameters, and checking for statistical significance among the distributions, split by dataset, age and sex, it was found, in line with previous research, that males tend to move more than females, regardless of which activity they are performing within the scanner. Similarly, it was shown that younger children tend to move more than older children, regardless of sex. Interestingly, the inclusion of active responses and multi-sensory stimulation in the Emotional N-Back Task fMRI scans was found to have a larger influence on male children, than female children, reducing the standard deviation of the distributions of all male displacement parameters. These findings may help guide future MR scans by putting extra focus on preparing male children to move less within the scanner.

Among the rotation displacement parameters, rotation around the x -axis, corresponding to nodding, was found to be the most influential parameter. This indicates, that future MRI preparation measures might benefit from training the children to avoid unnecessary nodding. Likewise, among the translation displacement parameters, translation along the y -axis, corresponding to sliding out of the bore, was found to be the most significant. Hence, future MRI scans might benefit from the inclusion of a non-slip mat, or duvet, to avoid sliding motions.

7 Code Availability

The code used for loading, preprocessing, and analysing the data can be found at GitHub: <https://github.com/melanieganz/MoCoProject/tree/1bcf4ce73d139b1d38a5cb8a1f7e34a77cfc957f/ChildrenHeadMotionABCD>.

References

- [1] *ABCD Study: About.* <https://abcdstudy.org/about/>. Accessed: 30-12-2023.
- [2] *ABCD Study: Full Baseline Data Demographics.* <https://abcdstudy.org/scientists/data-sharing/baseline-data-demographics-2-0/>. Accessed: 30-12-2023.
- [3] *ABCD Study: Protocols.* <https://abcdstudy.org/scientists/protocols/>. Accessed: 30-12-2023.

- [4] Onur Afacan et al. “Evaluation of motion and its effect on brain magnetic resonance image quality in children”. In: *Pediatric radiology* 46 (2016), pp. 1728–1735.
- [5] Betty Jo Casey et al. “The adolescent brain cognitive development (ABCD) study: imaging acquisition across 21 sites”. In: *Developmental cognitive neuroscience* 32 (2018), pp. 43–54.
- [6] Henrica MA De Bie et al. “Preparing children with a mock scanner training protocol results in high quality structural and functional MRI scans”. In: *European journal of pediatrics* 169 (2010), pp. 1079–1085.
- [7] Hannah Eichhorn et al. “Characterisation of children’s head motion for Magnetic Resonance Imaging with and without general anaesthesia”. In: *Frontiers in Radiology* 1 (2021), p. 789632.
- [8] Frank Godenschweger et al. “Motion correction in MRI of the brain”. In: *Physics in medicine & biology* 61.5 (2016), R32.
- [9] Mark Jenkinson et al. “Improved optimization for the robust and accurate linear registration and motion correction of brain images”. In: *Neuroimage* 17.2 (2002), pp. 825–841.
- [10] Reuben Mezrich. “A perspective on K-space”. In: *Radiology* 195.2 (1995), pp. 297–315.
- [11] National Institute of Biomedical Imaging and Bioengineering: *Magnetic Resonance Imaging (MRI)*. <https://www.nibib.nih.gov/science-education/science-topics/magnetic-resonance-imaging-mri>. Accessed: 30-12-2023.
- [12] Cynthia B Paschal and H Douglas Morris. “K-space in the clinic”. In: *Journal of Magnetic Resonance Imaging: An Official Journal of the International Society for Magnetic Resonance in Medicine* 19.2 (2004), pp. 145–159.
- [13] Jonathan D Power et al. “Spurious but systematic correlations in functional connectivity MRI networks arise from subject motion”. In: *Neuroimage* 59.3 (2012), pp. 2142–2154.
- [14] Maximilian F Reiser, Wolfhard Semmler, and Hedvig Hricak. *Magnetic resonance tomography*. Springer Science & Business Media, 2007.
- [15] Gregory G Slabaugh. “Computing Euler angles from a rotation matrix”. In: *Retrieved on August 6.2000* (1999), pp. 39–63.
- [16] Weihong Yuan et al. “Quantification of head motion in children during various fMRI language tasks”. In: *Human brain mapping* 30.5 (2009), pp. 1481–1489.
- [17] Maxim Zaitsev, Julian Maclarens, and Michael Herbst. “Motion artifacts in MRI: A complex problem with many partial solutions”. In: *Journal of Magnetic Resonance Imaging* 42.4 (2015), pp. 887–901.

8 Appendix

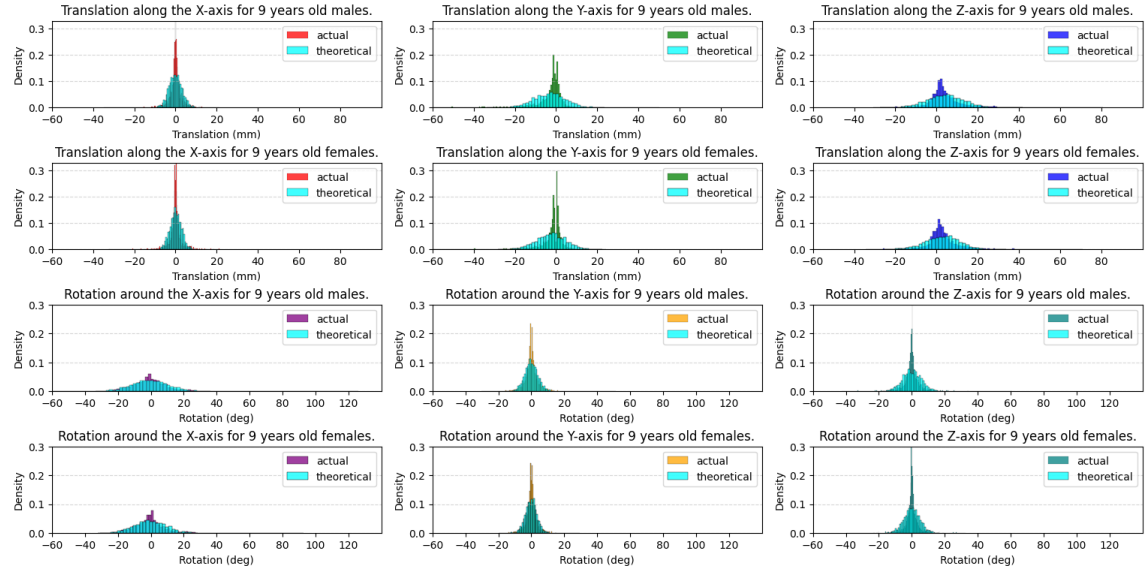


Figure 12: (rs-fMRI) Histogram of maximum absolute displacements for 9-year old children.

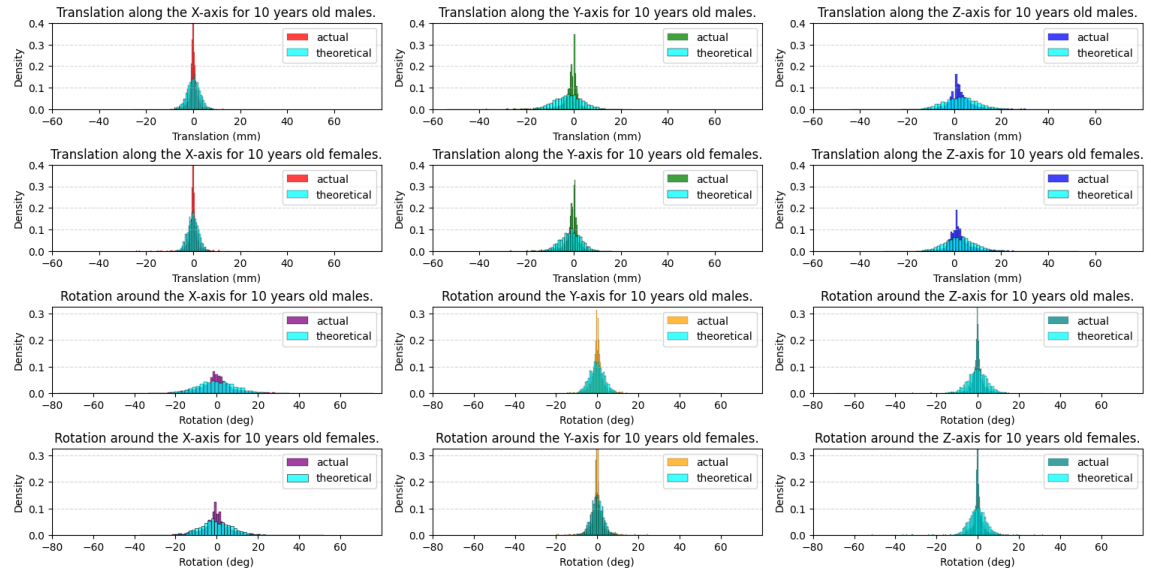


Figure 13: (rs-fMRI) Histogram of maximum absolute displacements for 10-year old children.

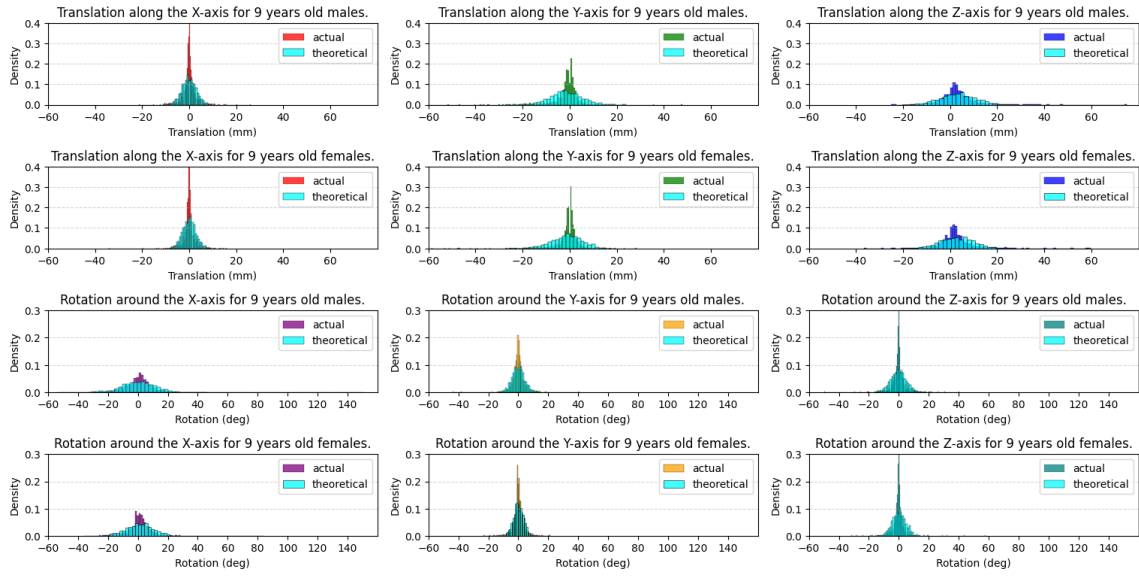


Figure 14: (EN-Back Task fMRI) Histogram of maximum absolute displacements for 9-year old children.

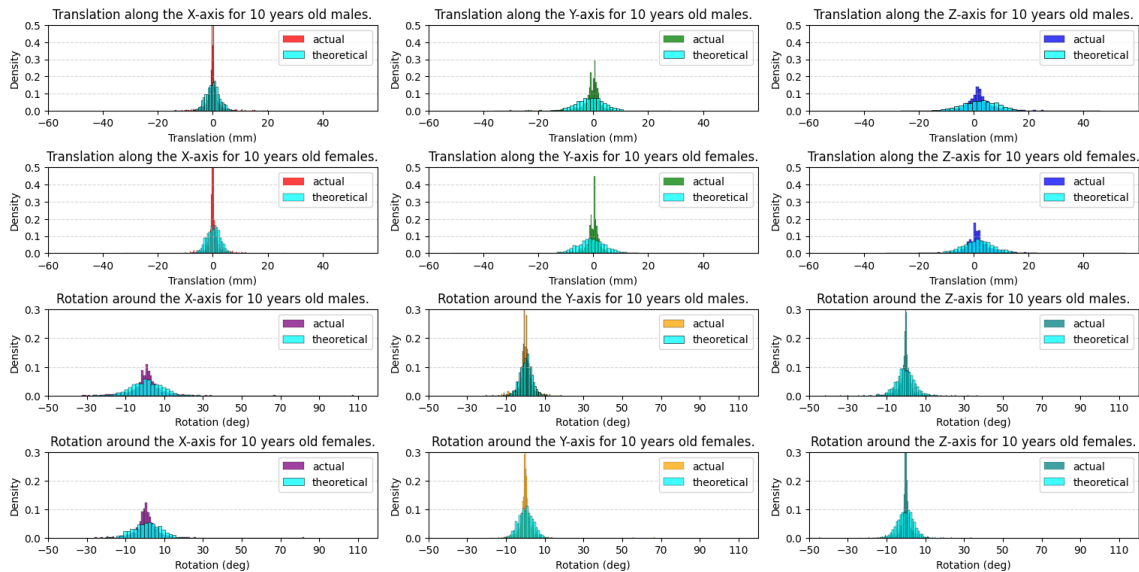


Figure 15: (EN-Back Task fMRI) Histogram of maximum absolute displacements for 10-year old children.

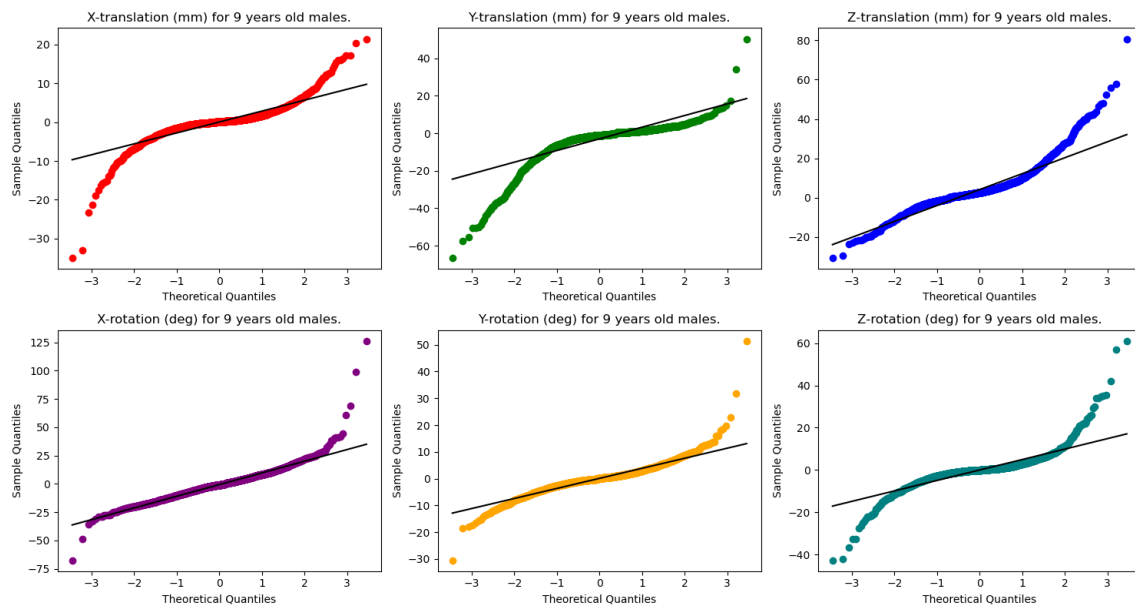


Figure 16: (rs-fMRI) Q-Q-plot for 9-year old males.

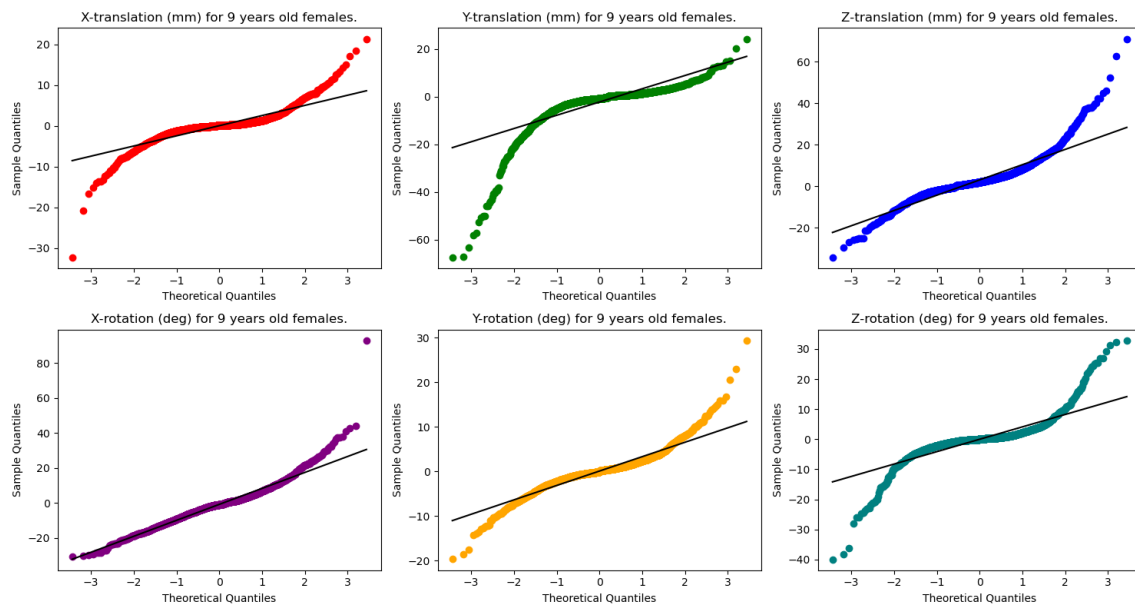


Figure 17: (rs-fMRI) Q-Q-plot plot for 9-year old females.

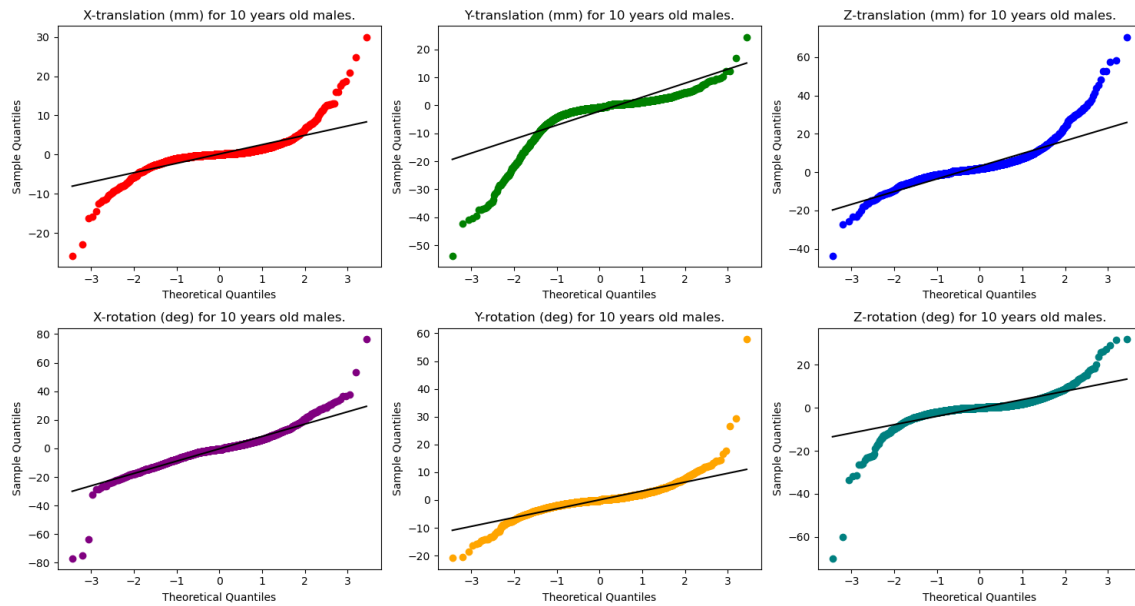


Figure 18: (rs-fMRI) Q-Q-plot plot for 10-year old males.

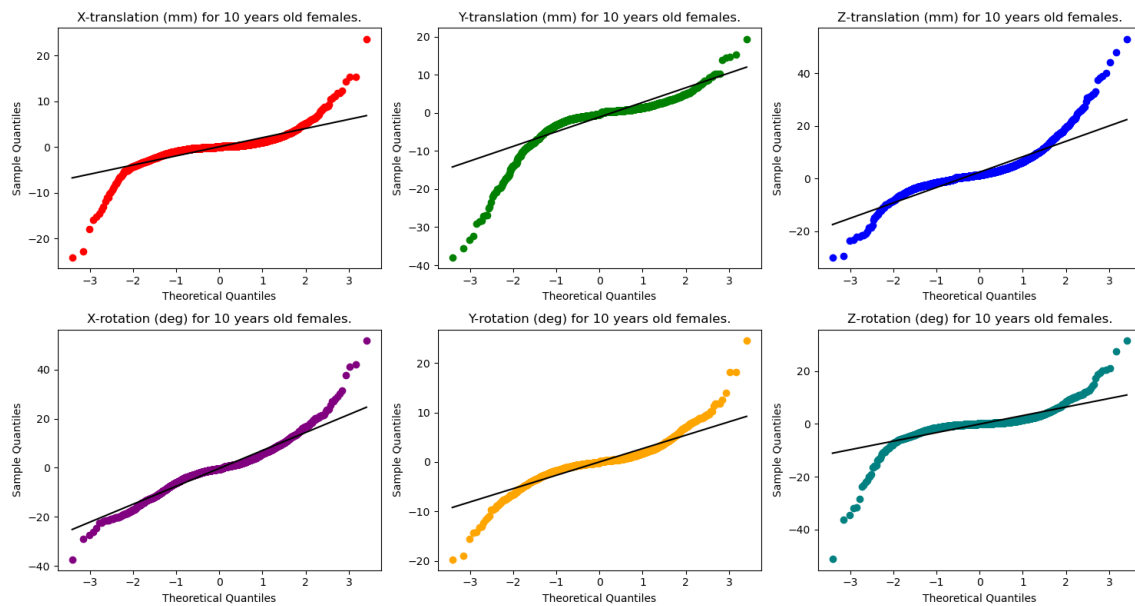


Figure 19: (rs-fMRI) Q-Q-plot plot for 10-year old females.